Cardiac ferroportin regulates cellular iron homeostasis and is important for cardiac function

Samira Lakhal-Littleton[a,1], Magda Wolna[a], Carolyn A. Carr[a], Jack J. J. Miller[a], Helen C. Christian[a], Vicky Ball[a], Ana Santos[b], Rebeca Diaz[b], Daniel Biggs[b], Richard Stillion[c], Philip Holdship[d], Fiona Larner[d], Damian J. Tyler[a], Kieran Clarke[a], Benjamin Davies[b], and Peter A. Robbins[a]

[a]Department of Physiology, Anatomy and Genetics, University of Oxford, Oxford OX1 3PT, United Kingdom; [b]Wellcome Trust Centre for Human Genetics, University of Oxford, Oxford OX3 7BH, United Kingdom; [c]Dunn School of Pathology, University of Oxford, Oxford OX1 3RF, United Kingdom; and [d]Department of Earth Sciences, University of Oxford, Oxford OX1 3AN, United Kingdom

Edited by William S. Sly, Saint Louis University School of Medicine, St. Louis, MO, and approved February 4, 2015 (received for review November 24, 2014)

Iron is essential to the cell. Both iron deficiency and overload impinge negatively on cardiac health. Thus, effective iron homeostasis is important for cardiac function. Ferroportin (FPN), the only known mammalian iron-exporting protein, plays an essential role in iron homeostasis at the systemic level. It increases systemic iron availability by releasing iron from the cells of the duodenum, spleen, and liver, the sites of iron absorption, recycling, and storage respectively. However, FPN is also found in tissues with no known role in systemic iron handling, such as the heart, where its function remains unknown. To explore this function, we generated mice with a cardiomyocyte-specific deletion of *Fpn*. We show that these animals have severely impaired cardiac function, with a median survival of 22 wk, despite otherwise unaltered systemic iron status. We then compared their phenotype with that of ubiquitous hepcidin knockouts, a recognized model of the iron-loading disease hemochromatosis. The phenotype of the hepcidin knockouts was far milder, with normal survival up to 12 mo, despite far greater iron loading in the hearts. Histological examination demonstrated that, although cardiac iron accumulates within the cardiomyocytes of *Fpn* knockouts, it accumulates predominantly in other cell types in the hepcidin knockouts. We conclude, first, that cardiomyocyte FPN is essential for intracellular iron homeostasis and, second, that the site of deposition of iron within the heart determines the severity with which it affects cardiac function. Both findings have significant implications for the assessment and treatment of cardiac complications of iron dysregulation.

iron | ferroportin | heart | cardiomyocyte | hepcidin

Iron is a constituent of hemoproteins, iron-sulfur proteins, and other functional groups that are essential for cellular functions. As such, effective iron homeostasis is essential to health in general and to cardiovascular health in particular. In the case of iron deficiency, two major randomized clinical trials have shown that even modest iron deficiency limits cardiac function in patients who have heart failure (1–3). Conversely, excess iron also is detrimental to cardiac function, as exemplified by cardiac failure of transfusional iron overload in patients with β-thalassemia and of primary iron overload in patients with hemochromatosis (4–6). The mechanisms linking excess cardiac iron with dysfunction involve both the production of cell-damaging free radicals through Fenton-type reactions (7, 8) and the electrophysiological changes caused by the competitive effects of ferrous iron on calcium signaling (4).

Ferroportin (FPN) is the only known mammalian iron-exporting protein (9) and is central to systemic iron homeostasis. It mediates iron release into the circulation from the duodenum, the splenic reticuloendothelial macrophages, and the liver, the sites of iron absorption, recycling, and storage, respectively (10–12). FPN-mediated iron release is antagonized by the hormone hepcidin antimicrobial peptide (HAMP). Produced primarily in the liver, HAMP binds to and induces internalization of FPN, thereby limiting iron release into the circulation and its availability to peripheral tissues (13–15).

As well as being expressed in the duodenum, the spleen, and the liver, tissues with a known role in systemic iron handling, FPN is found in other tissues with no such recognized role. One such tissue is the heart, where FPN is expressed in cardiomyocytes but where its function remains unexplored (16, 17).

The purpose of this study was to define the function of cardiac FPN. To do so, we first generated a conditional *Fpn* knockout allele in C57B6 mice which then was used to produce animals with a cardiomyocyte-specific deletion of *Fpn*. This approach enabled the study of the function of cardiac FPN on a background of otherwise intact systemic iron homeostasis. In addition, we generated an animal model of the iron-loading disease hemochromatosis by using an in-house conditional *Hamp* knockout allele to produce animals with a ubiquitous deletion of *Hamp*. We then compared the cardiac phenotypes of cardiac *Fpn* knockouts and ubiquitous *Hamp* knockouts.

Our findings in cardiac *Fpn* knockouts show that, in addition to its recognized role in systemic iron homeostasis, FPN regulates cellular iron homeostasis in cardiomyocytes in a manner that is critical to cardiac function. Furthermore, comparison between cardiac *Fpn* knockouts and ubiquitous *Hamp* knockouts demonstrates the importance of both cardiac FPN in determining the site of cardiac iron deposition and the site of deposition in determining the severity with which excess iron affects cardiac function.

Significance

The iron-exporting protein ferroportin is recognized as central to systemic iron regulation, but its role in tissues other than those involved in iron handling is unknown. This study shows that ferroportin expression in cardiomyocytes is essential to intracellular iron homeostasis and to normal cardiac function. It also demonstrates that the site of iron accumulation in the iron-overloaded heart depends on whether ferroportin is expressed in the cardiomyocytes. It further shows that the functional significance of cardiac iron overload is highly dependent upon the site of iron accumulation. These findings change our understanding of intracellular iron homeostasis and have significant implications for the clinical management of cardiac dysfunction associated with iron imbalance.

Author contributions: S.L.-L. and P.A.R. designed research; S.L.-L., M.W., H.C.C., A.S., R.D., D.B., R.S., and P.H. performed research; S.L.-L., C.A.C., J.J.J.M., H.C.C., V.B., A.S., R.D., D.B., F.L., D.J.T., K.C., and B.D. contributed new reagents/analytic tools; S.L.-L. analyzed data; and S.L.-L., B.D., and P.A.R. wrote the paper.

The authors declare no conflict of interest.

This article is a PNAS Direct Submission.

Freely available online through the PNAS open access option.

[1]To whom correspondence should be addressed. Email: samira.lakhal-littleton@dpag.ox.ac.uk.

This article contains supporting information online at www.pnas.org/lookup/suppl/doi:10.1073/pnas.1422373112/-/DCSupplemental.

Results

FPN Expression in the Heart and Its Regulation by Iron. In the adult mouse heart stained with anti-FPN antibody, FPN protein was observed in cardiomyocytes throughout the ventricular myocardium. FPN was localized predominantly to the cell membrane, although it also was present in the intracellular compartment in some cardiomyocytes (Fig. 1*A*).

In hearts from *Fpn fl/fl Myh6.Cre*$^{+}$ mice, cardiac FPN protein was undetectable (Fig. 1*A*), whereas FPN transcript levels were reduced by 85% relative to *Fpn fl/fl* controls (Fig. 1*B*). Nearly complete ablation of FPN expression in *Fpn fl/fl Myh6.Cre*$^{+}$ mice confirmed that cardiac FPN was expressed predominantly in cardiomyocytes, where Cre recombinase expression is driven specifically by the alpha myosin heavy-chain promoter. Liver FPN protein and RNA (Fig. 1 *A* and *B*, respectively) were not different in *Fpn fl/fl Myh6.Cre*$^{+}$ mice and *Fpn fl/fl* controls.

Consistent with the cardiac-specific deletion, *Fpn fl/fl Myh6.Cre*$^{+}$ mice had normal levels of liver iron stores and circulating iron indices as compared with *Fpn fl/fl* controls (Fig. 1*C*), demonstrating that loss of cardiac FPN did not alter systemic iron homeostasis.

Furthermore, we investigated the transcriptional regulation of Fpn by iron in vivo in wild-type C57B6 mice and in isolated adult cardiomyocytes. Compared with animals on control diet, cardiac Fpn transcript was reduced by the provision of an iron-deficient diet (iron 2–5 ppm) for 8 wk and was up-regulated by the provision of an iron-loaded diet (iron 5,000 ppm) for 6 wk (Fig. 1*D*).

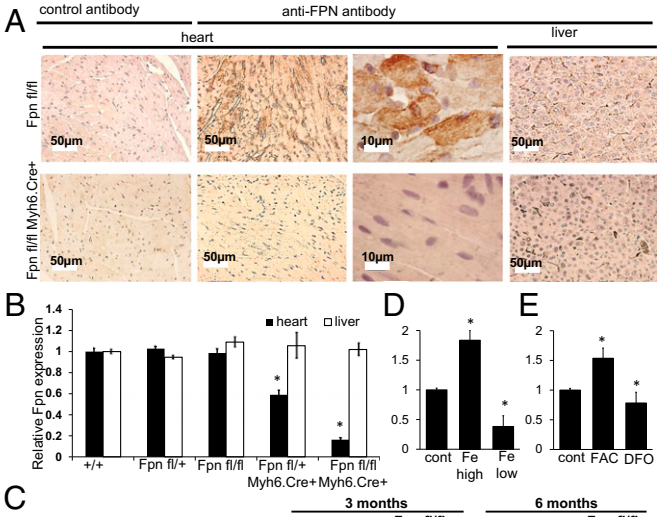

C

	3 months		6 months	
	Fpn fl/fl	Fpn fl/fl Myh6.Cre+	Fpn fl/fl	Fpn fl/fl Myh6.Cre+
Liver ferritin (ug/mg total protein)	1.60± 0.37	1.56± 0.19	1.96± 0.3	2.01± 0.36
Liver total elemental iron (ng/mg tissue)	14.6± 0.5	14.1± 0.5	13.6± 2.8	12.6± 3.0
Hb (g/L)	128.6± 3.2	121.3± 3.9	121.5± 2.2	123.3± 17.6
Serum ferritin (mg/L)	1.25± 2.02	1.27± 0.56	1.65± 0.33	1.58± 0.47
Serum iron(μmol/L)	31.5± 9.6	33.3± 6.5	34.9± 8.7	32.3± 10.3
Serum Tf (g/L)	0.63± 0.24	0.62± 0.19	0.69± 0.18	0.73± 0.21

Fig. 1. FPN expression in the heart and its regulation by iron. (*A*) Immunohistochemical staining for FPN in heart (ventricular myocardium) and liver sections from *Fpn fl/fl Myh6.Cre*$^{+}$ and *Fpn fl/fl* littermate control mice. (*B*) Relative expression of Fpn in hearts and livers of *Fpn*$^{+/+}$ (wild type), *Fpn fl/*$^{+}$ (heterozygous floxed), *Fpn fl/fl* (homozygous floxed), *Fpn fl/*$^{+}$ *Myh6.Cre*$^{+}$ (heterozygous cardiac knockout), and *Fpn fl/fl Myh6.Cre*$^{+}$ (homozygous cardiac knockout) mice. $n = 6$ per group determined by quantitative PCR. (*C*) Indices of iron homeostasis in the liver and circulation of *Fpn fl/fl Myh6.Cre*$^{+}$ mice and *Fpn fl/fl* littermate controls at age 3 and 6 mo. $n = 6$ per group. (*D*) Quantitative PCR expression of Fpn in hearts of wild-type C57B6 mice after 8 wk of a low-iron diet or 6 wk of a high-iron diet, relative to mice on the respective control diets. $n = 6$ per group. (*E*) Quantitative PCR expression of Fpn in isolated adult cardiomyocytes following 8-h treatment with ferric citrate (FAC) or deferoxamine (DFO). $n = 3$ biological replicates. All values are plotted as mean ± SEM. $^{*}P < 0.05$ relative to control.

Similarly, in cultured adult cardiomyocytes, Fpn expression was suppressed by the iron chelator deferoxamine and was up-regulated by addition of ferric citrate in the culture medium (Fig. 1*E*). These results demonstrate that cardiac Fpn transcription is regulated by iron.

Increased Mortality of *Fpn fl/fl Myh6.Cre*$^{+}$ Mice Is Associated with Gross Cardiac Abnormalities. To determine the effects of loss of cardiac FPN, we first assessed the cumulative survival of *Fpn fl/fl Myh6.Cre*$^{+}$ mice and *Fpn fl/fl* littermate controls over a period of 40 wk. Significantly greater mortality was observed among *Fpn fl/fl Myh6.Cre*$^{+}$ mice, with only 20% of animals surviving to 40 wk, compared with 85% of *Fpn fl/fl* controls. The median survival of *Fpn fl/fl Myh6.Cre*$^{+}$ mice was 22 wk, whereas the majority of *Fpn fl/fl* controls were still alive at the time of this report (9 mo) (Fig. 2*A*).

When animals died under observation, the heart was removed immediately and fixed for further histological examination. This examination showed significant enlargement of the left ventricular (LV) lumen and thinning of the LV wall in *Fpn fl/fl Myh6.Cre*$^{+}$ hearts compared with *Fpn fl/fl* controls (Fig. 2*B*). These hearts also had altered cellular morphology, with dilated cardiomyocytes and elongated nuclei (Fig. 2*B*). By electron microscopy, hearts from *Fpn fl/fl Myh6.Cre*$^{+}$ mice showed signs of myofibrillar disarray and an increased number of mitochondria in cardiomyocytes, not seen in hearts from *Fpn fl/fl* controls (Fig. 2*C*).

Dilated Cardiomyopathy with LV Dysfunction in *Fpn fl/fl Myh6.Cre*$^{+}$ Mice. To characterize further the phenotype caused by loss of cardiac FPN, we measured cardiac performance in vivo by cine MRI in anesthetized *Fpn fl/fl Myh6.Cre*$^{+}$ mice and *Fpn fl/fl* littermate controls at age 3 wk, 6 wk, 3 mo, and 6 mo. Cardiac function at age 3 and 6 wk was not different in *Fpn fl/fl Myh6.Cre*$^{+}$ mice and littermate controls (Fig. S1). At age 3 mo there was a marked and significant enlargement of the LV lumen in *Fpn fl/fl Myh6.Cre*$^{+}$ mice, both at end-systole and at end-diastole. This enlargement was accompanied by a 20% decrease LV ejection fraction (LVEF). At age 6 mo the increase in LV lumen was even greater and was associated with a 37% reduction in LVEF (Fig. 3*A*). Other parameters of cardiac performance were not altered significantly between mice from the two genotypes (Table S1). Examination of mid–ventricle cine MR images confirmed enlargement of the LV lumen in *Fpn fl/fl Myh6.Cre*$^{+}$ mice compared with *Fpn fl/fl* controls (Fig. 3*B*).

Taken together, histological examination of the hearts and cine MRI studies indicate that *Fpn fl/fl Myh6.Cre*$^{+}$ mice develop a phenotype consistent with dilated cardiomyopathy.

These changes in cardiac performance could not be attributed to Cre recombinase toxicity in the heart because *Myh6.Cre*$^{+}$ mice exhibited normal cardiac function at age 3 and 6 mo as compared with wild-type littermate controls (Table S2).

Increased Iron Content in Cardiomyocytes of *Fpn fl/fl Myh6.Cre*$^{+}$ Mice. Given the known function of FPN in iron export, we hypothesized that *Fpn fl/fl Myh6.Cre*$^{+}$ mice retain more iron within the heart. To test this hypothesis, we compared the cardiac iron content in *Fpn fl/fl Myh6.Cre*$^{+}$ and *Fpn fl/fl* controls at age 3 wk, 6 wk, 3 mo, and 6 mo. At age 3 wk cardiac iron content, as determined by ferritin and total elemental iron concentrations, was comparable in *Fpn fl/fl Myh6.Cre*$^{+}$ mice and *Fpn fl/fl* controls. In both sets of mice cardiac iron content increased gradually over time. However, the rate of this increase was greater in *Fpn fl/fl Myh6.Cre*$^{+}$ mice than in *Fpn fl/fl* littermate controls. At age 6 mo, ferritin and total elemental iron concentrations were 37% and 33% greater, respectively, in cardiac lysates from *Fpn fl/fl Myh6.Cre*$^{+}$ mice than in cardiac lysates from *Fpn fl/fl* controls (Fig. 4 *A* and *B*).

In addition, the magnetic resonance relaxation parameter T_2^* was significantly shorter in the myocardium of 6-mo-old *Fpn fl/fl*

SYSTEMS BIOLOGY

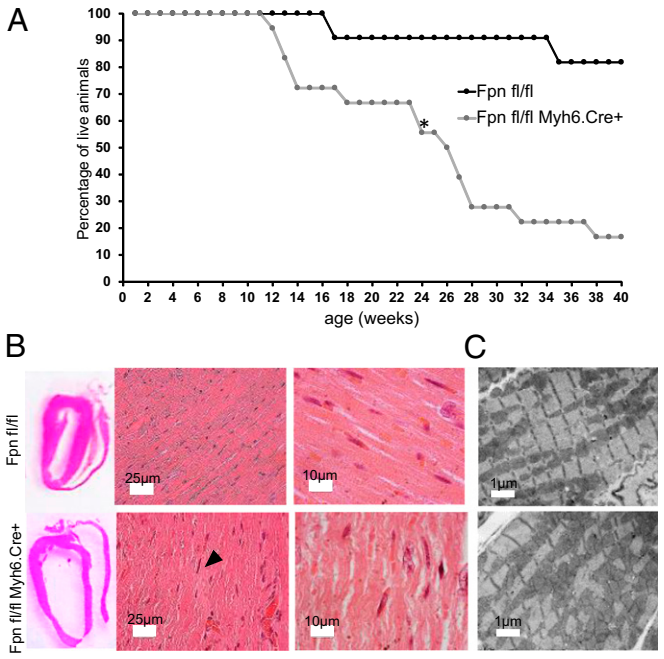

Fig. 2. Reduced survival of *Fpn fl/fl Myh6.Cre*$^{+}$ mice is associated with abnormal heart morphology. (*A*) Cumulative survival of *Fpn fl/fl Myh6.Cre*$^{+}$ mice and *Fpn fl/fl* littermates over 40 wk. *$P < 0.05$. $n = 20$ per group. (*B*) Representative images of gross morphology in longitudinal cardiac sections and cardiomyocyte histology in a 6-mo-old *Fpn fl/fl Myh6.Cre*$^{+}$ mouse (*Lower*) and an *Fpn fl/fl* littermate control (*Upper*). The arrowhead indicates an elongated nucleus. (*C*) Representative electron microscopy images of cardiac myofibril organization in *Fpn fl/fl* mice and *Fpn fl/fl Myh6.Cre*$^{+}$ mice at age 3 mo. Note the loss of myofibrillar regularity and increased mitochondrial numbers in cardiomyocytes in *Fpn fl/fl Myh6.Cre*$^{+}$ hearts.

Myh6.Cre^{+} mice than in controls, indicating an increase in cardiac iron content (Fig. 4*C*).

Next we examined the site of cardiac iron deposition in these mice. 3,3′-Diaminobenzidine (DAB)-enhanced Perls staining showed marked ferric iron deposits within the cardiomyocytes of *Fpn fl/fl Myh6.Cre*$^{+}$ mice, particularly at age 6 mo (Fig. 4*D*). Widespread deposition of electron-dense material (presumed to be iron) in lysosomes, around mitochondria, along sarcomeres, and within the dilated sarcoplasmic reticulum of *Fpn fl/fl Myh6.Cre*$^{+}$ cardiomyocytes was also observed by electron microscopy (Fig. 4*E*).

We also measured the cardiac levels of zinc, cobalt, copper, and manganese by inductively coupled plasma (ICP)-MS. There were no significant differences in the levels of these metals in *Fpn fl/fl* My6.Cre^{+} and *Fpn fl/fl* hearts, suggesting that these metals are not involved in the cardiac dysfunction observed in *Fpn fl/fl* My6.Cre^{+} mice (Fig. 4*F*).

To establish further the role of iron in the cardiac dysfunction seen in *Fpn fl/fl* My6.Cre^{+} mice, we determined the effects of dietary iron restriction on cardiac function and survival. When mice were provided with an iron-deficient diet (iron 2–5 ppm) for 8 wk after weaning, cardiac function in *Fpn fl/fl* My6.Cre^{+} mice no longer deteriorated at age 3 mo (Fig. 4*G*). Survival at the time of this report (6 mo) also was 100% for both *Fpn fl/fl Myh6.Cre*$^{+}$ and *Fpn fl/fl* mice.

Taken together, the observed deposition of iron but not other metals in the cardiomyocytes of *Fpn fl/fl Myh6.Cre*$^{+}$ mice and the cardioprotective effect of dietary iron restriction in these mice strongly implicate iron dysregulation in the phenotype associated with loss of cardiac FPN.

Differences in Cardiac Phenotype and Iron Deposition in *Fpn fl/fl Myh6.Cre*$^{+}$ and *Hamp*$^{-/-}$ Mice. Because the cardiac phenotype of *Fpn fl/fl Myh6.Cre*$^{+}$ mice was associated with increased cardiac iron content, we compared their phenotype with that of *Hamp*$^{-/-}$ mice, generated in-house as a model for the iron-loading disease hemochromatosis. We confirmed that the *Hamp*$^{-/-}$ mice that we generated had the expected elevated systemic iron indices, liver iron stores, and increased FPN expression in the liver and duodenum (Fig. S2 *A–C*). Cumulative 12-mo survival of *Hamp*$^{-/-}$ mice was not different from that of *Hamp*$^{+/+}$ littermate controls. Consistent with this finding, cine MRI demonstrated that cardiac performance was relatively spared in *Hamp*$^{-/-}$ mice, unlike that in *Fpn fl/fl Myh6.Cre*$^{+}$ mice. LV function was not significantly different in *Hamp*$^{+/+}$ and *Hamp*$^{-/-}$ mice, and on the right side *Hamp*$^{-/-}$ mice developed only a 20% increase in volume of the right ventricular (RV) lumen [but with preserved RV ejection fraction (RVEF)] at age 6 mo (Fig. S2*D*).

Ferritin and total elemental iron concentrations in cardiac lysates from *Hamp*$^{-/-}$ mice were elevated significantly relative to *Hamp*$^{+/+}$ controls, as is consistent with previously reported cardiac iron loading in humans and other animal models of hemochromatosis (Fig. 5*A*).

Interestingly, the degree of cardiac iron loading, as assessed by ferritin and elemental iron content, was much greater in *Hamp*$^{-/-}$ mice (~450% increase relative to *Hamp*$^{+/+}$ controls) than in *Fpn fl/fl Myh6.Cre*$^{+}$ mice (~30% increase relative to *Fpn fl/fl* controls). However, Perls iron staining showed that, although iron accumulated primarily within cardiomyocytes in *Fpn fl/fl Myh6.Cre*$^{+}$ hearts (Fig. 4*D*), ferric iron deposits in *Hamp*$^{-/-}$ hearts were localized primarily in noncardiomyocytic cells (Fig. 5*B*). Electron micrograph images of *Hamp*$^{-/-}$ hearts showed the presence of iron deposits in the endothelium and intracapillary leukocytes (Fig. 5*C*).

Concomitant with the pattern of iron deposition, cardiac immunostaining showed marked up-regulation of FPN on the surface of and within cardiomyocytes in *Hamp*$^{-/-}$ mice compared with *Hamp*$^{+/+}$ controls (Fig. 5*D*).

To compare the distribution of iron in these hearts further, we quantified total elemental iron in cardiomyocyte and noncardiomyocyte fractions isolated from *Fpn fl/fl Myh6.Cre*$^{+}$,

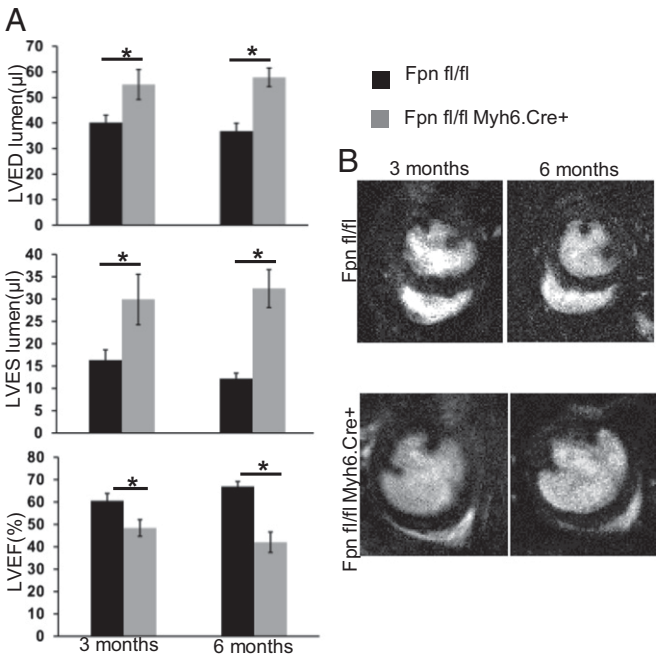

Fig. 3. Cardiac performance and morphology in vivo by cine MRI. (*A*) LV lumen size at end-systole (LVES) and end-diastole (LVED) and LVEF in *Fpn fl/fl Myh6.Cre*$^{+}$ mice and *Fpn fl/fl* controls at age 3 mo ($n = 12$ per group) and 6 mo ($n = 6$ per group). Values are plotted as mean ± SEM. *$P < 0.05$. (*B*) Representative midventricular MR images of hearts from *Fpn fl/fl Myh6.Cre*$^{+}$ mice and *Fpn fl/fl* controls at age 3 and 6 mo.

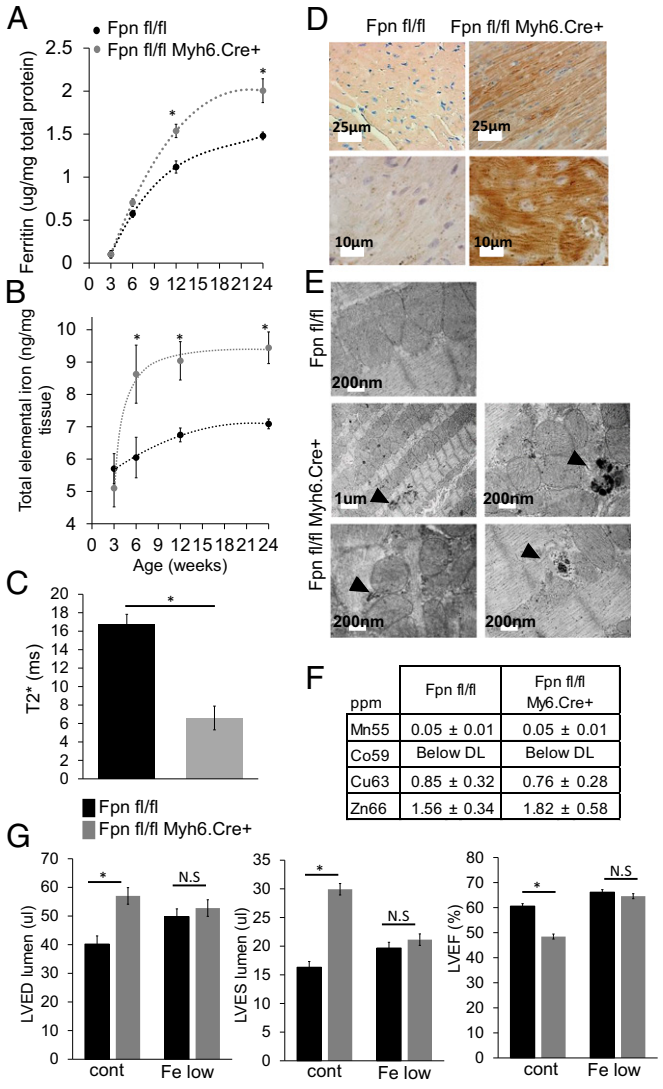

Fig. 4. Retention of iron in cardiomyocytes of *Fpn fl/fl Myh6.Cre*$^{+}$ mice. (*A*) Ferritin concentration in cardiac lysates from *Fpn fl/fl Myh6.Cre*$^{+}$ mice and *Fpn fl/fl* controls at age 3 wk ($n = 3$ per group), 6 wk ($n = 3$ per group), 3 mo ($n = 12$ per group), and 6 mo ($n = 6$ per group). (*B*) Total elemental iron concentration in cardiac lysates from *Fpn fl/fl Myh6.Cre*$^{+}$ mice and *Fpn fl/fl* controls at age 3 wk ($n = 3$ per group), 6 wk ($n = 3$ per group), 3 mo ($n = 12$ per group), and 6 mo ($n = 6$ per group). (*C*) T^{*}_{2} in *Fpn fl/fl Myh6.Cre*$^{+}$ mice and *Fpn fl/fl* controls at age 6 mo ($n = 6$ per group). (*D*) Representative images of DAB-enhanced Perls iron staining in ventricular myocardium from *Fpn fl/fl Myh6.Cre*$^{+}$ mice and *Fpn fl/fl* controls at age 6 mo. (*E*) Representative electron microscopy images of ventricular myocardium from 3-mo-old *Fpn fl/fl Myh6.Cre*$^{+}$ mice and *Fpn fl/fl* controls. Arrowheads indicate sites of iron deposition. (*F*) Levels of elemental zinc, cobalt, manganese, and copper in hearts of *Fpn fl/fl Myh6.Cre*$^{+}$ mice and *Fpn fl/fl* controls at age 6 mo ($n = 6$ per group); below DL, below detection limit. (*G*) Parameters of cardiac function as measured by cine MRI in 3-mo-old mice after 8 wk on the control diet or the low-iron diet ($n = 6$ per group). All values are plotted as mean ± SEM. *$P < 0.05$.

Hamp$^{-/-}$ hearts and their respective controls at age 6 mo. Results confirmed that, although total iron content was much greater in *Hamp*$^{-/-}$ hearts, the iron content of the cardiomyocyte fraction was greater in *Fpn fl/fl Myh6.Cre*$^{+}$ hearts (Fig. 5*E*).

Discussion

In the present study we demonstrate that, in addition to its well-recognized role in systemic iron homeostasis, FPN is important for cellular iron homeostasis in the heart. We show that loss of cardiac FPN results in rapid and ultimately fatal impairment of cardiac function in mice, associated with the deposition of iron within cardiomyocytes. These effects occur against a background of otherwise normal systemic iron homeostasis.

Iron enters cardiomyocytes primarily as transferrin (Tf), through transferrin receptor 1 (TfR1) but also can enter as non–Tf-bound iron (NTBI) through L-type calcium channels, T-type calcium channels, the divalent metal transporter DMT1, and the zinc transporter Zip14 (18–20). In the cell, excess iron is stored and detoxified in a protein complex called "ferritin" (21). TfR1 and ferritin expression is orchestrated in response to intracellular iron levels by the iron-regulatory proteins IRP1 and 2 (22, 23). IRPs sense intracellular iron through conformational change induced by the presence or absence of iron binding. IRP-dependent effects on iron uptake through TfR1 and on iron storage through ferritin are recognized as the primary mechanisms of cellular iron homeostasis. In *Fpn fl/fl Myh6.Cre*$^{+}$ hearts, TfR1 expression was down-regulated and L-ferrtin expression was up-regulated compared with *Fpn fl/fl* hearts, as is consistent with an intact IRP-mediated response to intracellular iron overload (Fig. S3). However, this IRP-mediated response did not prevent cardiac iron overload in these hearts. These results show that FPN-mediated iron export is an essential and nonredundant component of cellular iron homeostasis in cardiomyocytes. In this context, we have shown that cardiomyocyte FPN is itself regulated by iron levels, supporting the hypothesis that FPN is involved in maintaining cardiomyocyte iron balance under conditions of iron deficiency or overload. In addition to the posttranscriptional regulation of FPN by IRPs (22–24), there is posttranslational regulation by HAMP (Fig. 6*A*) (13–15). In the future, it would be interesting to examine formally both the relative contributions of IRPs and HAMP to the regulation of cardiac FPN and the

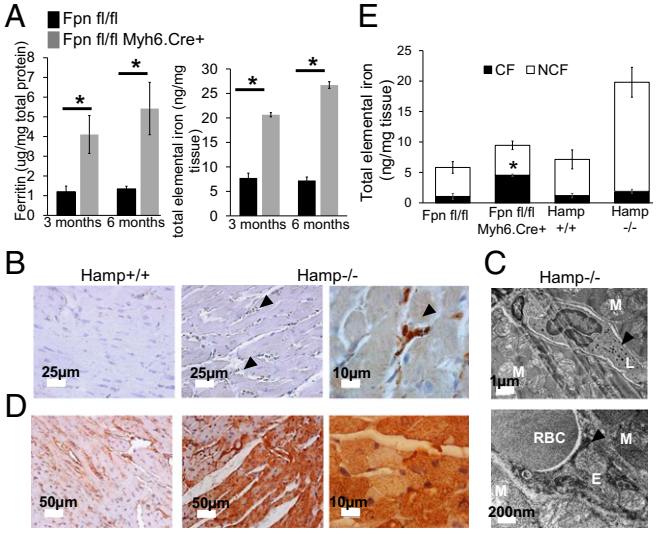

Fig. 5. Iron distribution in *Hamp*$^{-/-}$ mice. (*A*) Ferritin and total elemental iron concentrations in cardiac lysates from *Hamp*$^{-/-}$ mice and *Hamp*$^{+/+}$ controls at age 3 and 6 mo ($n = 12$ per group). *$P < 0.05$ relative to *Fpn fl/fl*. (*B*) Representative images of DAB-enhanced Perls staining in ventricular myocardium of *Hamp*$^{-/-}$ mice and *Hamp*$^{+/+}$ littermate controls at age 6 mo. Arrowheads indicate sites of iron accumulation. (*C*) Representative electron microscopy images of ventricular myocardium from 6-mo-old *Hamp*$^{-/-}$ mice. Arrowheads indicate sites of iron deposition. E, endothelial cell; L, leukocyte; M, myocyte; RBC, red blood cell. (*D*) Representative images of FPN immunohistochemical staining in ventricular myocardium of 6-mo-old *Hamp*$^{-/-}$ mice and *Hamp*$^{+/+}$ littermate controls. (*E*) Levels of elemental iron as measured by ICP-MS in cardiomyocyte fractions (CF) and noncardiomyocyte fractions (NCF) from hearts of 6-mo-old *Fpn fl/fl Myh6.Cre*$^{+}$ mice, *Hamp*$^{-/-}$ mice, and respective littermate controls ($n = 3$ per group). *$P < 0.05$ relative to cardiomyocyte fractions in *Hamp*$^{-/-}$ mice. Values are shown as mean ± SEM.

SYSTEMS BIOLOGY

interplay between iron uptake and iron release in cellular iron homeostasis using double-knockout mouse models. A further unanswered question is the degree to which our findings in cardiomyocytes generalize to other FPN-expressing tissues, e.g., kidney and brain (25, 26).

In this study we also compared the phenotype of *Fpn fl/fl Myh6.Cre*$^{+}$ mice with that of *Hamp*$^{-/-}$ mice, a recognized model of the iron-loading disease hemochromatosis. Despite a far greater degree of cardiac iron loading in *Hamp*$^{-/-}$ mice, the cardiac phenotype was much milder than that of *Fpn fl/fl Myh6.Cre*$^{+}$ mice, and survival up to 12 mo was unaffected. Histological examination revealed that cardiac iron was deposited within the cardiomyocytes in *Fpn fl/fl Myh6.Cre*$^{+}$ mice but primarily in noncardiomyocytic cells in *Hamp*$^{-/-}$ mice. This difference in the site of cardiac iron deposition is likely to be caused by the lack of cardiomyocyte FPN in the former setting and its marked up-regulation in the latter. Important conclusions stem from the comparisons of *Fpn fl/fl Myh6.Cre*$^{+}$ and *Hamp*$^{-/-}$ mice. First, the combination of normal iron uptake and impaired iron export (as in *Fpn fl/fl Myh6.Cre*$^{+}$ hearts) results in greater cardiomyocyte iron load than the combination of increased iron uptake and export (as in *Hamp*$^{-/-}$ hearts). Second, the site of iron deposition within the heart determines the severity with which it affects cardiac function. Third, expression of cardiac FPN is an important determinant of the site of cardiac iron deposition (Fig. 6*B*).

In contrast to *Fpn fl/fl Myh6.Cre*$^{+}$ mice, patients with ferroportin disease, an inherited disorder of iron metabolism caused by dominant loss of FPN function, have not been reported to have cardiac complications (27, 28). However, although *Fpn fl/fl Myh6.Cre*$^{+}$ mice retain intact FPN function in the duodenum, liver, and reticuloendothelial system, patients with ferroportin disease do not, leading to iron accumulation in the spleen and liver, reduced circulating Tf and NTBI, and marginal anemia (28). Given the known role of NTBI in cardiac iron overload, it is plausible that decreased NTBI entry into cardiomyocytes in these patients offsets the iron-loading effects of loss of cardiac FPN. This hypothesis is supported by our finding that dietary iron restriction protects *Fpn fl/fl Myh6.Cre*$^{+}$ mice from developing cardiac dysfunction.

The lack of significant cardiac dysfunction in our *Hamp*$^{-/-}$ mice and in other reported mouse models of impaired hepcidin production (29–31) is in contrast with the clinical characteristics of juvenile hemochromatosis, in which patients develop severe cardiomyopathy (5). This contrast points to possible differences between human and murine cardiomyocytes in iron entry, export, storage, or detoxification pathways. In the context of iron overload, the entry of NTBI into cardiomyocytes is recognized as a contributor to cardiac iron loading and subsequent dysfunction (18–20). Therefore, interesting questions are whether known NTBI transporters differ in human and mouse cardiomyocytes and whether such differences account for the divergent cardiac phenotypes.

Despite these differences in the human and murine settings, the basic mechanistic understanding of iron regulation in cardiomyocytes, of which FPN is an essential component, is valuable in the clinical setting. Indeed, our findings highlight the need to assess carefully the impact of iron-manipulation therapies on the distribution as well as the amount of iron deposited within the heart. They also suggest that targeted up-regulation of cardiac FPN may present therapeutic opportunities in cardiac complications of iron overload.

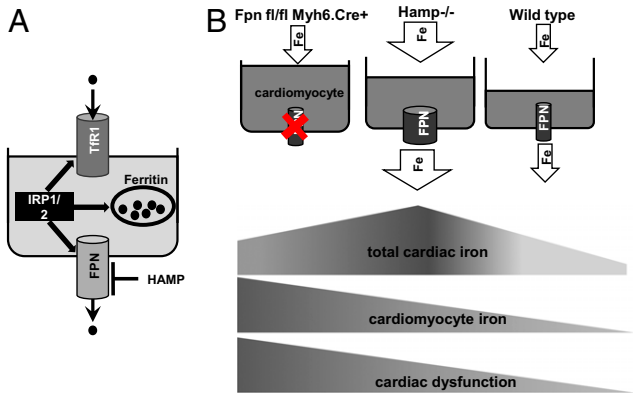

Fig. 6. The role of FPN in cardiac iron homeostasis. (*A*) Integrated model of cellular iron homeostasis. FPN in cardiomyocytes is central to their cellular iron homeostasis. Together with TfR1-mediated iron uptake and ferritin storage, it controls iron levels within cardiomyocytes. FPN itself is regulated by intracellular iron levels in a manner dependent on IRP1 and IRP2 and by hepcidin derived from the liver and/or the heart itself. (*B*) FPN determines the site of cardiac iron deposition and the severity of the associated cardiac phenotype. Cardiomyocyte iron homeostasis occurs at the point of balance between iron entry and iron efflux. Because FPN is the only known mammalian iron-export protein, its expression in cardiomyocytes promotes iron efflux and a reduction in intracellular iron content. Loss of cardiomyocyte FPN leads to a severe cardiac phenotype, despite a mild degree of total cardiac iron loading. Up-regulation of FPN in *Hamp*$^{-/-}$ mice appears to be protective against the effects of systemic iron overload by enabling the release of iron from cardiomyocytes.

Materials and Methods

Generation of Mouse Models. All animal procedures were compliant with and approved by both the UK Home Office Animals (Scientific Procedures) Act 1986 and the University of Oxford Medical Sciences Division Ethical Review Committee.

***Cardiac* Fpn *knockouts*.** The strategy for the generation of cardiac *Fpn* knockout mice is outlined in Fig. S4. Briefly, C57BL/6N mice harboring a knockout first mutation at the *Fpn* (*Slc40a1*) locus were obtained from the European Mouse Mutant Cell Consortium and were crossed with a C57BL/6 Flp recombinase deleter mouse, Tg(ACTB-FlpE)9205Dym/J, to remove the selection cassette and generate a *Fpn* allele with floxed exons 4 and 5, which encode the transmembrane domain. As a first line of validation, we crossed floxed mice (*Fpn fl/fl*) with mice transgenic for the ubiquitously expressed Pgk1-Cre recombinase, Tg(Pgk1-cre) (32), and confirmed embryonic lethality in ubiquitous homozygous knockouts (*Fpn*$^{-/-}$). Cardiac *Fpn* knockouts then were generated by crossing homozygous *Fpn fl/fl* animals with mice transgenic for Myh6-Cre recombinase B6.FVB-Tg(Myh6-cre)2182Mds/J (33), which is under the control of cardiomyocyte-specific myosin alpha heavy-chain 6 promoter. The subsequent breeding strategy was designed to produce cardiac *Fpn* knockouts and homozygous floxed controls (hereafter referred to as "*Fpn fl/fl Myh6.Cre*$^{+}$" and "*Fpn fl/fl*," respectively) in the same litter.

***Ubiquitous Hamp knockouts*.** The strategy for generating *Hamp*-knockout mice is outlined in Fig. S5. Briefly, a targeting vector was designed to introduce a floxed *Hamp* allele into mouse ES cells, with exons 2 and 3, which encode the majority of the peptide, flanked by LoxP sites. Further breeding with a C57BL/6 Flp recombinase deleter mouse allowed removal of the Neomycin resistance cassette. Heterozygous *Hamp* knockouts were generated by crossing floxed *Hamp* animals with Pgk1-Cre transgenic mice. *Hamp*$^{-/-}$ animals and *Hamp*$^{+/+}$ littermate controls were obtained from *Hamp*$^{+/-}$ crossings.

Study Design. *Fpn fl/fl Myh6.Cre*$^{+}$ mice, *Hamp*$^{-/-}$ mice, and their respective littermate controls *Fpn fl/fl* and *Hamp*$^{+/+}$ were housed under standard animal housing conditions in individually ventilated cages. They were assessed for cardiac function by cine MRI at age 3 wk, 6 wk, 3 mo, or 6 mo, and then were culled for assessment of systemic and cardiac iron indices.

Dietary Iron Content. Unless otherwise stated, animals were supplied a standard rodent chow diet containing 200 ppm iron. In iron-deficiency experiments, mice were provided an iron-deficient diet (2–5 ppm iron; Teklad TD.99397; Harlan Laboratories) or a matched control diet (200 ppm iron; Teklad TD.08713) from weaning for 8 wk. In iron-overload experiments, 8- to 10-wk-old mice were provided an iron-loaded diet (5,000 ppm iron; Teklad TD.140464) or a matched control diet (200 ppm iron; Teklad TD.08713) for 6 wk.

Isolated Adult Cardiomyocyte Experiments. Adult cardiomyocytes were isolated from 8-wk-old wild-type C57B6 mice as described in *SI Materials and Methods*. Within 2 h of cardiomyocyte culture, cells were treated with

0.5 mM ferric citrate (F3388; Sigma Aldrich) or 100 uM deferoxamine (D9533; Sigma Aldrich) for 8 h.

Cine MRI. Mice were anesthetized with 2% (vol/vol) isofluorane in O_2 and were positioned supine in a purpose-built cradle. Cine MR imaging was carried out using an 11.7-T MR system with a 40-mm birdcage coil (Rapid Biomedical) as described (34) and summarized in *SI Materials and Methods*.

T_2^*. Mice were anesthetized with 2% (vol/vol) isofluorane in O_2 and positioned supine in a purpose-built cradle. All experiments were performed on a 7-T preclinical MRI system (Agilent Technologies) as described in *SI Materials and Methods*.

Quantitative PCR. Total RNA was extracted from frozen mouse tissues using the RNAeasy kit (Qiagen) and was reverse-transcribed into cDNA using M-MLV-reverse transcriptase (Ambion) and poly-dT primers. cDNA then was used as template in duplex quantitative real-time PCR reactions using Taqman gene expression assay probes for Fpn, TfR1, and L-ferritin, and the housekeeping gene *β-actin* (Life Technologies).

Immunohistochemistry and DAB-Enhanced Perls Staining. Formalin-fixed paraffin-embedded tissues were sectioned into 0.5-μm sections and stored at room temperature. Sections were deparaffinized using xylene and then were rehydrated in ethanol before being subjected to heat-activated antigen retrieval in citrate buffer (pH 6). Slides then were blocked for nonspecific binding using protein block, and endogenous peroxidase activity was quenched. For immunohistochemistry, slides were stained with rabbit polyclonal anti-mouse FPN antibody (Alpha Diagnostics) and then were developed using the Dako Envision HRP-DAB System. For DAB-enhanced Perls staining, slides were immersed for 1 h in 1% potassium ferricyanide in 0.1 M HCl buffer and then were stained with DAB chromogen substrate. All slides were counterstained with hematoxylin and then were visualized using a standard brightfield microscope.

Electron Microscopy. Hearts were dissected, and 0.5- to 1-mm^3 slices were fixed by immersion for 2 h in 2.5% (wt/vol) glutaraldehyde in 0.1 M cacodylate buffer and were prepared for electron microscopy by standard methods. Briefly, cells were postfixed in osmium tetroxide [1% (wt/vol) in 0.1 M phosphate buffer], stained with uranyl acetate [2% (wt/vol) in distilled water], dehydrated through increasing concentrations of ethanol (70–100%) and acetone, and embedded in TAAB resin (TAAB Laboratories Equipment, Ltd.). Ultrathin sections (50–80 nm) were prepared using a Reichert Ultracut S microtome and were mounted on 200-mesh nickel grids. Sections were lightly counterstained with lead citrate and uranyl acetate and were examined with a Jeol transmission electron microscope (JEM-1010; JEOL).

Isolation of Cardiomyocyte and Noncardiomyocyte Fractions for Iron Quantitation. Following cardiac perfusion, hearts were dissected into small pieces in ice-cold Hanks buffer and were subjected to collagenase P digestion at 37 °C for 1 h (11213857001; Roche Diagnostics). Following lysis of red blood cells, cell suspensions were passed through a 70-um sieve before being labeled using a cardiomyocyte isolation kit (130-100-825; Miltenyi Biotec). Separation of cardiomyocyte and noncardiomyocyte fractions was carried out using a MACS magnetic separation system (Miltenyi Biotec) according to the manufacturer's instructions. Fractions were lysed immediately for ICP-MS analysis.

Iron Quantitation. The ferritin concentration in cardiac and liver lysates was determined using a ferritin ELISA kit (ICL, Inc.) and was normalized to total protein concentration. Serum ferritin levels also were determined by the same ELISA kit. Serum iron and Tf levels were determined using the ABX-Pentra system (Horiba Medical). To determine total elemental iron and other metals in the heart and the liver, tissues were heat-digested completely in nitric acid and then were prepared for ICP-MS. Measurements were carried out as described in *SI Materials and Methods*. Iron quantitation was carried out in washed, nonperfused hearts. We confirmed that the same results with respect to iron levels were obtained when using perfused hearts (Fig. S6).

Statistical Analysis. Values are shown as mean ± SEM. Comparison of iron indices and parameters of cardiac function between groups was performed using Student's *t* test. *P* values <0.05 were deemed as indicating significant differences between groups.

ACKNOWLEDGMENTS. We thank Dr. Oliver Lomas and Ms Marcella Brescia, Oxford University, for their assistance with cardiac perfusions. This work was funded by the British Heart Foundation and Vifor Pharma.

1. Anker SD, et al.; FAIR-HF Trial Investigators (2009) Ferric carboxymaltose in patients with heart failure and iron deficiency. *N Engl J Med* 361(25):2436–2448.
2. Okonko DO, et al. (2008) Effect of intravenous iron sucrose on exercise tolerance in anemic and nonanemic patients with symptomatic chronic heart failure and iron deficiency FERRIC-HF: A randomized, controlled, observer-blinded trial. *J Am Coll Cardiol* 51(2):103–112.
3. Klip IT, et al. (2013) Iron deficiency in chronic heart failure: An international pooled analysis. *Am Heart J* 165(4):575–582, e3.
4. Lekawanvijit S, Chattipakorn N (2009) Iron overload thalassemic cardiomyopathy: Iron status assessment and mechanisms of mechanical and electrical disturbance due to iron toxicity. *Can J Cardiol* 25(4):213–218.
5. Murphy CJ, Oudit GY (2010) Iron-overload cardiomyopathy: Pathophysiology, diagnosis, and treatment. *J Card Fail* 16(11):888–900.
6. Allen KJ, et al. (2008) Iron-overload-related disease in HFE hereditary hemochromatosis. *N Engl J Med* 358(3):221–230.
7. Walter PB, et al. (2006) Oxidative stress and inflammation in iron-overloaded patients with beta-thalassaemia or sickle cell disease. *Br J Haematol* 135(2):254–263.
8. Young IS, et al. (1994) Antioxidant status and lipid peroxidation in hereditary haemochromatosis. *Free Radic Biol Med* 16(3):393–397.
9. Ganz T (2005) Cellular iron: Ferroportin is the only way out. *Cell Metab* 1(3):155–157.
10. Donovan A, et al. (2005) The iron exporter ferroportin/Slc40a1 is essential for iron homeostasis. *Cell Metab* 1(3):191–200.
11. Donovan A, et al. (2000) Positional cloning of zebrafish ferroportin1 identifies a conserved vertebrate iron exporter. *Nature* 403(6771):776–81.
12. McGregor JA, et al. (2005) Impaired iron transport activity of ferroportin 1 in hereditary iron overload. *J Membr Biol* 206(1):3–7.
13. Nemeth E, et al. (2004) Hepcidin regulates cellular iron efflux by binding to ferroportin and inducing its internalization. *Science* 306(5704):2090–2093.
14. Qiao B, et al. (2012) Hepcidin-induced endocytosis of ferroportin is dependent on ferroportin ubiquitination. *Cell Metab* 15(6):918–924.
15. Ross SL, et al. (2012) Molecular mechanism of hepcidin-mediated ferroportin internalization requires ferroportin lysines, not tyrosines or JAK-STAT. *Cell Metab* 15(6):905–917.
16. Abboud S, Haile DJ (2000) A novel mammalian iron-regulated protein involved in intracellular iron metabolism. *J Biol Chem* 275(26):19906–19912.
17. Ge XH, et al. (2009) The iron regulatory hormone hepcidin reduces ferroportin 1 content and iron release in H9C2 cardiomyocytes. *J Nutr Biochem* 20(11):860–865.
18. Oudit GY, Trivieri MG, Khaper N, Liu PP, Backx PH (2006) Role of L-type Ca2+ channels in iron transport and iron-overload cardiomyopathy. *J Mol Med (Berl)* 84(5):349–364.
19. Kumfu S, Chattipakorn S, Chinda K, Fucharoen S, Chattipakorn N (2012) T-type calcium channel blockade improves survival and cardiovascular function in thalassemic mice. *Eur J Haematol* 88(6):535–548.
20. Liuzzi JP, Aydemir F, Nam H, Knutson MD, Cousins RJ (2006) Zip14 (Slc39a14) mediates non-transferrin-bound iron uptake into cells. *Proc Natl Acad Sci USA* 103(37):13612–13617.
21. Worwood M (1990) Ferritin. *Blood Rev* 4(4):259–269.
22. Rouault TA (2006) The role of iron regulatory proteins in mammalian iron homeostasis and disease. *Nat Chem Biol* 2(8):406–414.
23. Rouault T, Klausner R (1997) Regulation of iron metabolism in eukaryotes. *Curr Top Cell Regul* 35(35):1–19.
24. McKie AT, et al. (2000) A novel duodenal iron-regulated transporter, IREG1, implicated in the basolateral transfer of iron to the circulation. *Mol Cell* 5(2):299–309.
25. Wolff NA, et al. (2011) Ferroportin 1 is expressed basolaterally in rat kidney proximal tubule cells and iron excess increases its membrane trafficking. *J Cell Mol Med* 15(2):209–219.
26. Moos T, Rosengren Nielsen T (2006) Ferroportin in the postnatal rat brain: Implications for axonal transport and neuronal export of iron. *Semin Pediatr Neurol* 13(3):149–157.
27. Babitt JL, Lin HY (2011) The molecular pathogenesis of hereditary hemochromatosis. *Semin Liver Dis* 31(3):280–292.
28. Pietrangelo A (2004) The ferroportin disease. *Blood Cells Mol Dis* 32(1):131–138.
29. Nicolas G, et al. (2001) Lack of hepcidin gene expression and severe tissue iron overload in upstream stimulatory factor 2 (USF2) knockout mice. *Proc Natl Acad Sci USA* 98(15):8780–8785.
30. Lesbordes-Brion JC, et al. (2006) Targeted disruption of the hepcidin 1 gene results in severe hemochromatosis. *Blood* 108(4):1402–1405.
31. Meynard D, et al. (2009) Lack of the bone morphogenetic protein BMP6 induces massive iron overload. *Nat Genet* 41(4):478–481.
32. Lallemand Y, Luria V, Haffner-Krausz R, Lonai P (1998) Maternally expressed PGK-Cre transgene as a tool for early and uniform activation of the Cre site-specific recombinase. *Transgenic Res* 7(2):105–112.
33. Agah R, et al. (1997) Gene recombination in postmitotic cells. Targeted expression of Cre recombinase provokes cardiac-restricted, site-specific rearrangement in adult ventricular muscle in vivo. *J Clin Invest* 100(1):169–179.
34. Tyler DJ, et al. (2006) CINE-MR imaging of the normal and infarcted rat heart using an 11.7 T vertical bore MR system. *J Cardiovasc Magn Reson* 8(2):327–333.